Renewable Energy 224 (2024) 120178

Contents lists available at ScienceDirect

Renewable Energy

journal homepage: www.elsevier.com/locate/renene

Improved production of methyl levulinate from catalytic conversion of cellulose over cobalt sulfide by nickel doping

Gang Wu [a,1], Ke Wang [a], Shasha Liu [b,1], Shanshan Yan [a], Kuan Ding [a], Electo Eduardo Silva Lora [c], Yusuf Makarfi Isa [d], Yong Huang [a], Shu Zhang [a,*]

[a] Joint International Research Laboratory of Biomass Energy and Materials, Jiangsu Co-Innovation Center of Efficient Processing and Utilization of Forest Resources, College of Materials Science and Engineering, Nanjing Forestry University, Nanjing, 210037, Jiangsu, China
[b] School of Intelligent Manufacturing, Nanjing Polytechnic Institute, Nanjing, 210044, Jiangsu, China
[c] Mechanical Engineering Institute, Federal University of Itajuba, Ave. BPS 1303 CP CEP 37500-083, Brazil
[d] School of Chemical and Metallurgical Engineering, University of the Witwatersrand, Johannesburg, 2050, South Africa

ARTICLE INFO

Keywords:
Methyl levulinate
Bimetallic sulfide
Nickel doping
Solid acid catalyst

ABSTRACT

Transition metal sulfides have rich Brønsted/Lewis's acid sites and various metal valence states, which have great influence on their catalytic performance. In this study, the nickel cobalt sulfides with different molar ratios of Ni to Co were synthesized by one-step solvothermal method for the highly efficient catalytic conversion of cellulose into methyl levulinate (ML). Interestingly, with the continuous incorporation of Ni, the catalytic efficiency of the catalysts increased first and then decreased. It was worth mentioning that when the ratio of Co/Ni is 1, the ML yield was the highest (39.6 wt%), much higher than CoS_2 and NiS_2 (30.5 and 30.1 wt%, respectively). Based on the characterization of the prepared catalysts, it was found that the improved catalytic performance of $Ni_{0.50}Co_{0.50}S_2$ was potentially due to the synergistic effect of lower Co^{3+}/Co^{2+} ratio and larger Ni^{3+}/Ni^{2+} ratio. Furthermore, the $Ni_{0.50}Co_{0.50}S_2$ catalyst had a great recycling performance, which still maintained 78% of the initial catalytic efficiency after reused for 5 times.

1. Introduction

With the rapid consumption of conventional fossil energy and continuous deterioration of ecological environment, the development of renewable energy is urgent [1]. Biomass, as the fourth largest energy resource in the world, has the advantages of rich resources, wide distribution, renewability and so on [1–3]. In addition, biomass is also a renewable carbon-containing resource, which plays an extremely important role in the production of carbon-based materials [4].

It is widely known that lignocellulosic biomass abundant in nature is composed by three main components, i.e., cellulose, hemicellulose, and lignin, of which the contents are in ranges of 40–60, 15–30, and 10–25 wt%, respectively [5]. Thus, the efficient conversion of the cellulose fraction has always been the focus of biomass research due to its abundant and renewable reserves [6]. The conversion of cellulose into high value-added fuels and platform chemicals is a promising way to turn waste or trash into treasure and reduce the reliance on fossil fuel resources [7].

Cellulose can be used as a raw material to prepare a series of high value-added platform chemicals through catalytic conversion such as gluco-oilgomers [8], glucose [9], maltose [10], HMF [11], 2,5-HD [12], formic acid [13], LG [14] and levulinic acid (LA) through various depolymerization reactions [15]. In the past decades, these platform chemicals have been prepared directionally by researchers, especially LA, which has attracted extensive attention due to its excellent chemical properties [16]. In addition, LA derivatives have attracted much attention due to the usage as organic solvents, spices, paints and fuel additives, and methyl levulinate (ML) is one of the most important representative chemicals of LA derivatives [17].

Catalysts used for the directional preparation of ML from cellulose include liquid acid catalysts, ion liquid catalysts and solid acid catalysts [9]. There are some shortcomings in liquid acid catalysts and ionic liquid catalysts, such as difficult separation from products, corrosion of equipment, poor recycling performance, pollution to the environment, etc., which limit their widespread utilization [18], while solid acid catalysts have better stability, recycling performance and easier

* Corresponding author.
E-mail address: s.zhang@njfu.edu.cn (S. Zhang).
[1] Equal contribution to this work.

https://doi.org/10.1016/j.renene.2024.120178
Received 12 January 2023; Received in revised form 11 January 2024; Accepted 18 February 2024
Available online 19 February 2024

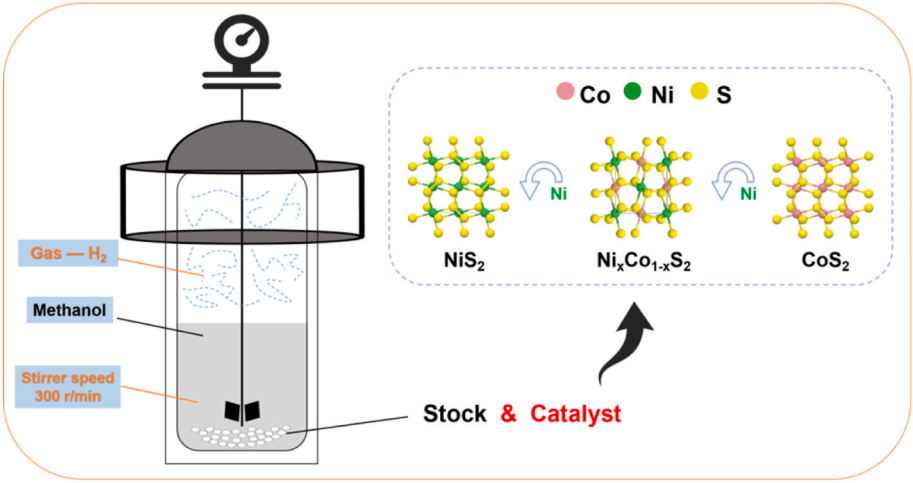

Fig. 1. Schematic diagram of using $Ni_xCo_{1-x}S_2$ as the catalysts for preparing ML in Micro HTHP Reactor.

recovery [19]. Heterogeneous catalysis using solid acid catalysts has been proved to be a highly active, more stable, and environmental-friendly production method [20]. Solid acid catalysts include zeolite, metal oxide and metal sulfide etc. [21]. Compared with zeolite and metal oxides, metal sulfides have attracted more attention due to their better thermal stability and mechanical properties, higher conductivity and higher redox reversibility [22].

To date, there are many transition metal sulfides such as ZnS [23], CoS_2 [24], FeS_2 [25], MoS_2 [26] and CuS [27] were widely explored as high performance solid acid catalysts materials. In our previous study, CoS_2 was designed as a single transition metal sulfide catalyst to prepare ML from cellulose with a yield of 30 wt%, focusing on the effect of Co valence states on the catalytic reaction pathways [28]. However, the surface active sites and conductivity of transition metal sulfides are limited by the single metal component. On the other hand, bimetallic sulfides can provide richer redox reactions and higher conductivity due to the synergistic effect of two transition metals [29]. Nickel and cobalt have similar electronic structures and chemical properties [30]. Therefore, nickel cobalt bimetallic sulfide can be used as a new catalyst with great potential for catalytic applications.

Herein, nickel cobalt sulfides, as environmentally friendly solid acid catalysts, with different molar ratios of Ni to Co were synthesized by one-step solvothermal method for the highly efficient catalytic conversion of cellulose to ML. Furthermore, the roles of the various physicochemical properties of the catalysts including micro-morphology, surface area, pore structure, crystal structure, surface functional groups, surface acid sites and metal valence states in the catalytic depolymerization of cellulose to prepare ML were investigated and understood, and the involved catalytic effects were revealed.

2. Experimental

2.1. Materials

Cellulose (50 μm, >99.9%), cobalt chloride hexahydrate ($CoCl_2{\cdot}6H_2O$, >99.9%), nickel chloride hexahydrate ($NiCl_2{\cdot}6H_2O$, >99.9%), and HPLC grade standard of ML ($C_6H_{10}O_3$, >99.9%) were purchased from Aladdin BioChem Technology Co. Ltd. in Shanghai, China. Sodium thiosulfate ($Na_2S_2O_3$, >99.9%) was purchased from Macklin Biochemical Co. Ltd. in Shanghai, China. Analytical grade methanol (CH_4O, > 99.5%) and ethanol (C_2H_6O, >99.9%) were purchased from Nanjing Chemical Reagent Co., Ltd. in Nanjing, China. High purity nitrogen (N_2, >99.999%) and high purity hydrogen (H_2, >99.999%) were purchased from Nanjing Special Gas Co., Ltd. in Nanjing, China. All chemicals were used without further purification.

2.2. Synthesis of catalysts

First of all, $CoCl_2{\cdot}6H_2O$ (4.76, 3.57, 3.19, 2.38, 1.57, 1.19 and 0 g), $NiCl_2{\cdot}6H_2O$ (0, 1.19, 1.57, 2.38, 3.19, 3.57 and 4.75 g), and $Na_2S_2O_3$ (4.74 g) were dissolved in 60 mL of deionized water and stirred evenly with a glass rod, and then treated with ultrasonic vibration for 30 min to obtain transparent solution. Whereupon, these obtained transparent solutions were transferred to the stainless-steel reactor with PTFE lining. After sealing and replacing the internal air with N_2, the reactor was heated to 200 °C for 12 h with a stirring rate of 200 rpm. When the reactor was cooled to room temperature, the filtered black powder solid product was alternately washed with ethanol and deionized water for more than 5 times, and then dried in a vacuum oven at 70 °C for 12 h to obtain the final black solid product. Finally, according to the amounts of $CoCl_2{\cdot}6H_2O$ and $NiCl_2{\cdot}6H_2O$ employed mentioned above, corresponding to different molar ratios (3:1, 2:1, 1:1, 1:2 and 1:3) of Co to Ni, the catalysts were labeled as $Ni_{0.25}Co_{0.75}S_2$, $Ni_{0.33}Co_{0.67}S_2$, $Ni_{0.50}Co_{0.50}S_2$, $Ni_{0.67}Co_{0.33}S_2$, or $Ni_{0.75}Co_{0.25}S_2$, respectively. In addition, catalysts without $NiCl_2{\cdot}6H_2O$ and without $CoCl_2{\cdot}6H_2O$ were labeled as CoS_2 and NiS_2, respectively.

2.3. Conversion of cellulose to ML over $Ni_xCo_{1-x}S_2$ ($0 \leq x \leq 1$) catalysts

First of all, 0.5 g of cellulose (dried at 70 °C), 20.0 mL of analytical grade methanol, and 0.1 g of CoS_2, $Ni_{0.25}Co_{0.75}S_2$, $Ni_{0.33}Co_{0.67}S_2$, $Ni_{0.50}Co_{0.50}S_2$, $Ni_{0.67}Co_{0.33}S_2$, $Ni_{0.75}Co_{0.25}S_2$ or NiS_2 catalysts were added to a 100 mL stainless steel autoclave. Then, the reactor was sealed and N_2 was used to replace the air in the reactor for 5 times. After the N_2 in the reactor was replaced with H_2 5 times, the autoclave was pressurized to a given pressure (2 MPa) at room temperature with H_2. It was then heated to the reaction temperature (200 °C) at 300 rpm mechanical stirring and kept at that temperature for 3 h (See Fig. 1). After cooled to room temperature by immersing in ice water, the autoclave was opened and the resulting solid liquid mixture was separated by vacuum filtration to collect the solid and liquid phases for subsequent characterization. All tests were repeated more than three times until the difference between the results was guaranteed to be less than 1%.

The resulting separated solid phase was washed with ethanol and deionized water alternately for several times to remove possible organic compounds and water-soluble substances, and then dried to a constant weight at 105 °C. In the catalyst durability tests, the dried solid product was calcined in a muffle furnace at 450 °C for 1 h to remove coke and insoluble humins, then washed with ethanol and deionized water, and dried to a fixed weight at 105 °C to obtain the recovered catalyst for the next catalytic test.

The resulting liquid phase product was diluted to 25 mL in a volumetric flask by methanol, and the chemicals in the liquid phase were qualitatively and quantitatively analyzed by gas chromatography/mass spectrometry (GC/MS) with a gas chromatograph (GC, Agilent 7890A, USA) coupled to a mass spectrometer (MSD, Agilent 5975C, USA). A commercial capillary column (Agilent J&W VF-1701 ms, 30 m length × 0.25 μm film thickness × 0.25 mm inner diameter) was employed for separation of compounds with the following temperature history: temperature maintaining at 40 °C for 2 min, heating to 200 °C at a rate of 5 °C·min^{-1}, raising to 280 °C at a rate of 10 °C·min^{-1}, and holding at 280 °C for 3 min. Meanwhile, the temperature of the auxiliary heating region connecting the chromatographic column end to the mass spectrometer detector was maintained at 285 °C. The injection volume was 1 μL with a split ratio of 20:1 and the MSD was operated in an electron impact mode at an ionization energy of 70 eV and with a scan range of m/z = 50−300. The interpretation of the mass spectra was based on library search (NIST11, version 2.0). The conversion of cellulose and the yield of ML were calculated by Equations (1) and (2).

$$Conversion\ (\%) = \frac{m_{feedstock} - m_{solid\ product}}{m_{feedstock}} \times 100\% \quad (1)$$

$$Yield\ (wt\%) = \frac{C \times V}{m_{feedstock}} \times 100\% \quad (2)$$

where *Conversion* (%) is the conversion of cellulose, $m_{feedstock}$ (g) is the mass of the raw feedstock, $m_{solid\ product}$ (g) is the mass of the solid product excluding the catalyst mass, *Yield* (wt%) is the mass yield of product, *C* (g/mL) is the concentration of product detected by GC/MS, and *V* (mL) is the total volume of liquid sample taken for GC/MS analysis.

2.4. Characterization of catalysts

The microstructures, morphologies and element distribution of the catalysts were observed using a scanning electron microscope under E-t secondary electron detector (SEM, ZEISS Sigma 300, Germany) coupled with energy-dispersive X-ray spectroscopy (EDS, ZEISS Sigma 300, Germany).

The textures of the catalysts were characterized via an isotheral nitrogen adsorbed/desorbed device, and the BrunauerEmmett-Teller (BET) method was used to calculate the parameters (e.g., the specific surface area, pore volume and pore size). After degassing at 150 °C for 12 h to remove the impurities, the textual properties of the catalysts were evaluated with an isothermal nitrogen adsorption/desorption analyzer (BSD-PM4, Beishide Instrument Technology Co., Ltd).

The crystalline structures of the catalysts were analyzed by X-ray diffraction (XRD) in the range of 10–80° at a scanning speed of 10°·min^{-1} using a Smartlab 9kw advance powder X-ray diffractometer (Rigaku, Japan) equipped with a Cu Ka (λ = 1.5406 Å) radiation source at 40 kV and 40 mA.

The types of functional groups were analyzed by a fourier transform infrared spectrometer (FT-IR, Bruker Vertex80V, Germany). The catalysts were prepared using the KBr technique, where about 200:1 ($mass_{(KBr)}$: $mass_{(catalyst)}$) was mixed in an agate mortar and then pelletized. The spectra was recorded in a range of 400–4000 cm^{-1} and scanned 16 times.

The acid sites were measured by temperature-programmed desorption of ammonia (NH_3-TPD) technique (PAC-1200 type, Beijing Peter Electronic Technology Co. Ltd. China). Prior to the test, the catalysts were treated at 200 °C under N_2 atmosphere for 2 h and saturated using 10 vol% NH_3 (30 mL min^{-1}) at 50 °C for 1 h. After purging by N_2 (30 mL min^{-1}) at 50 °C for 1 h, the NH_3-TPD was conducted by raising the temperature from 50 to 650 °C at a rate of 10 °C·min^{-1} and keeping it at 650 °C for 10 min under N_2 flow (30 mL min^{-1}).

X-ray photoelectron spectroscopy (XPS) was conducted in Thermo Scientific K-Alpha Nexsa (Thermo Scientific, UK) equipped with Al Kα radiation (1486.6 eV, 72 W) as the excitation source at a beam current of 15 mA to detect the chemical valences of cobalt, sulfur and phosphorus in the catalysts. The wide pass energy is 200 eV and the narrow pass energy is 50 eV. All XPS peaks were calibrated by the C 1s signal at 284.8 eV.

Table 1
The conversion of cellulose and the product yield over the different catalysts under the conditions of 200 °C, 2 MPa of initial pressure, and 3 h.

Entry	Catalyst	ML yield (wt%)	Conversion (%)
1	None	0	0
2	CoS_2	30.5 ± 0.5	96
3	$Ni_{0.25}Co_{0.75}S_2$	34.1 ± 0.2	98
4	$Ni_{0.33}Co_{0.67}S_2$	36.2 ± 0.3	100
5	$Ni_{0.50}Co_{0.50}S_2$	39.6 ± 0.2	100
6	$Ni_{0.67}Co_{0.33}S_2$	34.8 ± 0.2	99
7	$Ni_{0.75}Co_{0.25}S_2$	32.0 ± 0.1	97
8	NiS_2	30.1 ± 0.1	95
9	$Ni_{0.50}Co_{0.50}S_{2\ cycle\text{-}2}$	35.5	99
10	$Ni_{0.50}Co_{0.50}S_{2\ cycle\text{-}3}$	32.9	98
11	$Ni_{0.50}Co_{0.50}S_{2\ cycle\text{-}4}$	32.5	98
12	$Ni_{0.50}Co_{0.50}S_{2\ cycle\text{-}5}$	30.8	95

3. Results and discussion

3.1. Conversion of cellulose to ML over $Ni_xCo_{1-x}S_2$ catalysts

To further understanding and investigation the effect of $Ni_xCo_{1-x}S_2$ catalysts on cellulose depolymerization, various $Ni_xCo_{1-x}S_2$ catalysts were prepared by a one-pot solvothermal method. The conversion of cellulose in methanol over various $Ni_xCo_{1-x}S_2$ catalysts was therefore carried out under the conditions of 200 °C, H_2 atmosphere (2 MPa), and 3 h, which had been optimized in our previous study [31].

Table 1 summarizes the conversion of cellulose and ML yield over $Ni_xCo_{1-x}S_2$ catalysts. As a blank test without catalyst (Entry 1), legitimately, the conversion rate of cellulose and the yield of ML were both 0. The CoS_2 without Ni doping, as a single transition metal sulfide catalyst, unsurprisingly, enabled the conversion of cellulose and ML yield as high as 96% and 30.5 wt%, respectively (Entry 2). When Ni was doped into CoS_2 ($Ni_{0.25}Co_{0.75}S_2$, to $Ni_{0.33}Co_{0.67}S_2$, and to $Ni_{0.50}Co_{0.50}S_2$) with the Co/Ni atomic ratio ranging from 3, to 2, and to 1, the conversion of cellulose increased from 98% to 100%, and the ML yield significantly improved from 34.1, to 36.2, and to 39.6 wt%, respectively (Entries 3–5). Nevertheless, with the further doping of Ni into CoS_2 ($Ni_{0.50}Co_{0.75}S_2$, to $Ni_{0.67}Co_{0.33}S_2$, and to $Ni_{0.75}Co_{0.25}S_2$), as the Ni/Co atomic ratio increased from 1, to 2, and to 3, the conversion of cellulose decreased from 100%, to 99%, and to 97%, and the ML yield gradually reduced from 39.6, to 34.8, and to 32.0 wt%, respectively (Entries 5–7). In addition, when NiS_2 was used as catalyst, the conversion of cellulose and the yield of ML were the lowest, which were 95% and 30.1 wt%, respectively (Entry 8). It was not difficult to find that the catalytic efficiency of two single transition metal sulfide catalysts (CoS_2 and NiS_2) had little difference, and both were lower than that of double transition metal sulfide catalysts.

Based on the above results, there was no doubt that $Ni_{0.50}Co_{0.50}S_2$ had proved to be highly selective for ML formation and thus has great potential for industrial application in cellulose or lignocellulosic biomass conversion. As another significant factor for catalyst required in industry, the recyclability and stability of $Ni_{0.50}Co_{0.50}S_2$ were investigated here. As shown in Entries 9–12 of Table 1, the yields of ML from the $Ni_{0.50}Co_{0.50}S_2$ catalyzed runs slightly reduced from 39.6 (fresh catalyst) to 35.5, to 32.9, to 32.5, and finally to 30.8 wt% with the recycling number. In other words, the ML yield still accounted for 78% of the initial yield after the fifth recycling of the $Ni_{0.50}Co_{0.50}S_2$ catalyst, which implies that the recycling performance of the $Ni_{0.50}Co_{0.50}S_2$ catalyst was great. More importantly, the conversion of cellulose could be maintained at 95% after five cycles. Therefore, the $Ni_{0.50}Co_{0.50}S_2$

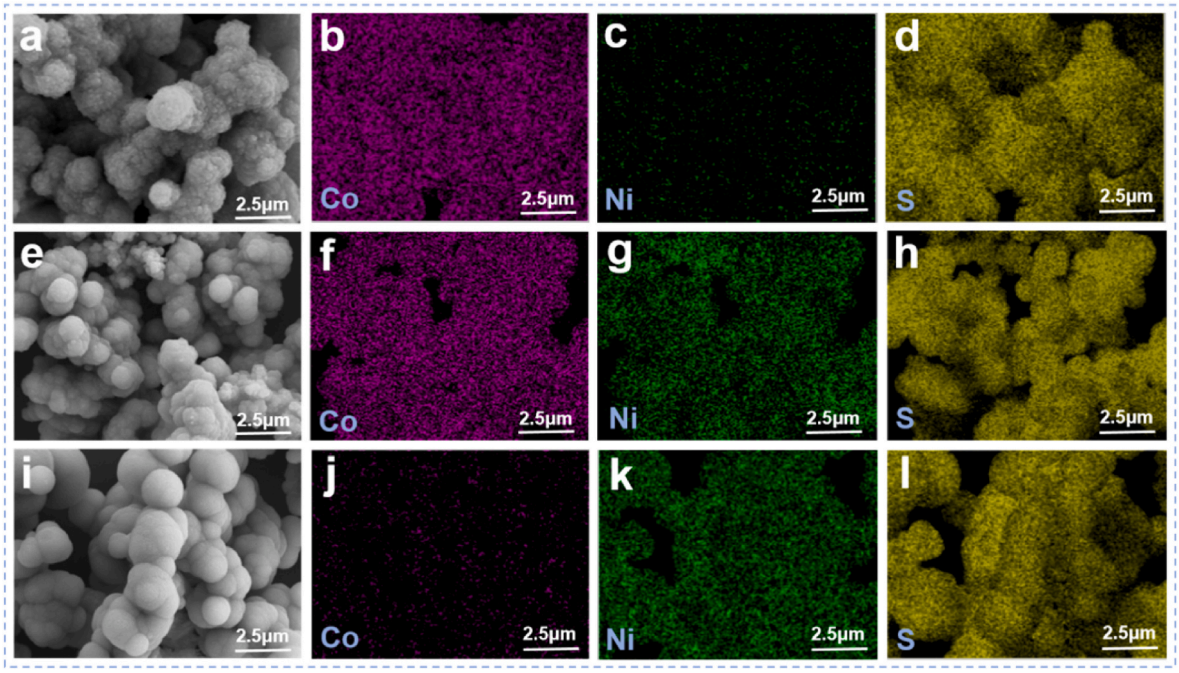

Fig. 2. SEM and EDS spectra of CoS_2 (a, b, c and d), $Ni_{0.50}Co_{0.50}S_2$ (e, f, g and h) and NiS_2 (i, j, k and l) catalysts.

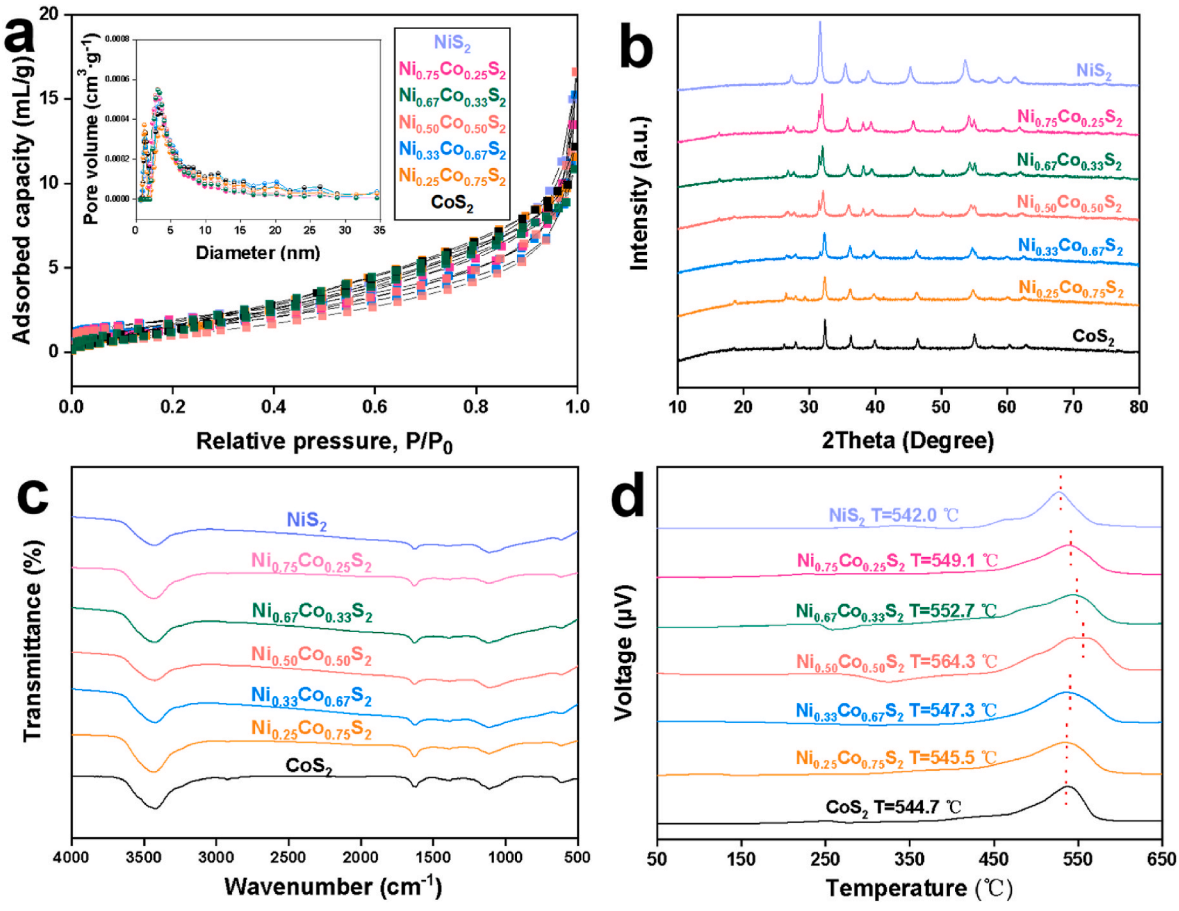

Fig. 3. The Nitrogen adsorption-desorption isotherms and pore size distribution (a), XRD patterns (b) and FT-IR(c), and NH_3-TPD analyses (d) of the catalysts.

Table 2
The porous parameters of the nickel cobalt sulfide catalysts.

Sample	Specific surface area ($m^2 \cdot g^{-1}$)	Pore volume ($cm^3 \cdot g^{-1}$)	Average pore size (nm)
CoS_2	9.0068	0.0242	10.7474
$Ni_{0.25}Co_{0.75}S_2$	8.5466	0.0294	10.9972
$Ni_{0.33}Co_{0.67}S_2$	8.6312	0.0237	11.5832
$Ni_{0.50}Co_{0.50}S_2$	8.5265	0.0219	10.8616
$Ni_{0.67}Co_{0.33}S_2$	8.9540	0.0212	11.8509
$Ni_{0.75}Co_{0.25}S_2$	8.7373	0.0236	11.4425
NiS_2	8.8337	0.0208	11.8336

catalyst exhibited a high stability during cellulose conversion to ML and had high potentials in largescale application as a new solid acid catalyst.

3.2. The effect of physicochemical properties of $Ni_xCo_{1-x}S_2$ catalyst on the preparation of ML

To understand the effect of nickel doping, various characterizations of $Ni_xCo_{1-x}S_2$ were conducted. The micro morphology of the catalysts has been reported to have an important impact on its catalytic performance [32]. Therefore, SEM analysis was used to explore possible differences among the micro morphologies of the catalysts. Fig. 2 exhibits the SEM images of three typical catalysts (CoS_2, $Ni_{0.50}Co_{0.50}S_2$, and NiS_2).

In addition, it was obvious that all of the $Ni_xCo_{1-x}S_2$ catalysts were characterized by imperfect spherical structures with a particle size of around 1–3 μm, which indicated that the morphology of CoS_2 was insignificantly changed by the doping of nickel and was not the key factor for the differences in their catalytic performance. From the SEM-EDS elemental mappings, it could be clearly seen that Co, Ni, or S were evenly distributed in the corresponding catalysts, proving the successful preparation of the designed $Ni_xCo_{1-x}S_2$ catalysts. More importantly, SEM-EDS elemental mappings semi quantitative test was also used to determine the proportions of Co, Ni, and S elements in the catalysts. As listed in Table S1, the detected atomic ratios of Co, Ni, and S elements were highly close to the theoretical values.

In many studies, the specific surface area and pore size distribution of catalysts played a direct and decisive role in their catalytic performances [33]. In order to investigate the effect of the specific surface area and pore structure, Fig. 3a shows the nitrogen adsorption and desorption isotherms of $Ni_xCo_{1-x}S_2$ catalysts, and no significant difference among them was found. All of the catalysts were characterized by small specific surface areas, which were in the range of 8.5265 $m^2\ g^{-1}$ ($Ni_{0.50}Co_{0.50}S_2$) to 9.0068 $m^2\ g^{-1}$ (CoS_2). The pore diameters of the catalysts were mainly distributed around 2.0 nm and 4.5 nm (Fig. 3a). Nevertheless, this was not the case in the present study since all the specific surface area, total pore volume, and average pore size of these catalysts had no obvious differences (Table 2). Consequently, the improved activity of $Ni_{0.50}Co_{0.50}S_2$ was not due to the change in the textural structures of CoS_2 or NiS_2.

XRD patterns obtained from the catalysts were shown in Fig. 3b. It could be clearly found that all of the catalysts had sharp crystal structures, and no impurities existed in these catalysts. The CoS_2 catalyst had sharp diffraction peaks at around $2\theta = 28.0$, 32.5, 36.4, 40.1, 46.6, 55.3, 58.0, 60.6, 63.1, 75.4, 77.8, and 79.8°, respectively attributing to the crystal facets (111), (200), (210), (211), (220), (311), (222), (230), (321), (331), (420), and (421) (PDF#41–1471) [34]. Meanwhile, the NiS_2 catalyst also had sharp diffraction peaks at around $2\theta = 27.1$, 31.4, 35.3, 38.8, 45.0, 53.4, 56.0, 58.5, 60.9, 72.4, 74.6, and 76.7°, respectively attributing to the crystal facets (111), (200), (210), (211), (220), (311), (222), (230), (321), (331), (420), and (421) (PDF#88–1709) [35]. Compared with the CoS_2, the main characteristic diffraction peaks of the NiS_2 catalyst did not obviously change except that the 2theta position corresponding to NiS_2 crystal had shifted to the left as a whole, which is mainly due to the larger cell volume and crystal plane spacing of NiS_2 crystal. Furthermore, it was worth noting that the $Ni_{0.50}Co_{0.50}S_2$ catalyst also had sharp crystal structure containing the crystal peaks of CoS_2 and NiS_2 (JCPDS card no.04-001-6119) [36]. The above results also demonstrated that $Ni_xCo_{1-x}S_2$ catalyst were successfully prepared. Furthermore, the relative contents of each crystal surface of the catalysts in the range of 2theta (0–80°) were shown in Table S2. No obvious difference in the crystal facet contents could be found among the catalysts, suggesting that the improved catalytic performance of $Ni_{0.50}Co_{0.50}S_2$ was not attributed to a specific crystal facet.

Table 3
The yield of ML prepared from cellulose in different reported reports.

Entry	Catalyst	Yield of ML/wt%	Ref.
1	A-CoS_2	28.9	[28]
2	Syn-CoS_2	30.5	[28]
3	CoS_2-1	31.7	[31]
4	CoS_2	30.5	This work
5	$Ni_{0.25}Co_{0.75}S_2$	34.1	
6	$Ni_{0.33}Co_{0.67}S_2$	36.2	
7	$Ni_{0.50}Co_{0.50}S_2$	39.6	
8	$Ni_{0.67}Co_{0.33}S_2$	34.8	
9	$Ni_{0.75}Co_{0.25}S_2$	32.0	
10	NiS_2	30.1	

Table 4
Peak position and amounts of NH_3 desorbed from the seven catalysts' sites, as determined using NH_3-TPD.

Sample	Peak position of the peak (°C)	Desorption peak area (a.u.)
CoS_2	544.7	5587
$Ni_{0.25}Co_{0.75}S_2$	545.5	6430
$Ni_{0.33}Co_{0.67}S_2$	547.3	6511
$Ni_{0.50}Co_{0.50}S_2$	564.3	7678
$Ni_{0.67}Co_{0.33}S_2$	552.7	7185
$Ni_{0.75}Co_{0.25}S_2$	549.1	6406
NiS_2	543.0	5381

Meanwhile, as is well known, the thermal stability of the cyclic catalysts is one of the important indicators for evaluating their performance. Based on this, XRD testing was used to investigate the thermal stability of the catalysts. Fig. S1 shows the comparison between the $Ni_{0.50}Co_{0.50}S_2$ before reaction and after 5 cycles of use. It is not difficult to find that the difference between their components and phases can be ignored, which indicated that the $Ni_{0.50}Co_{0.50}S_2$ has excellent heat resistance and cyclic stability. In addition, as shown in Table 3, the yields of ML prepared from cellulose in different reports (Previously reported works and this work) are compared. Meanwhile, as shown in Table S3, the catalytic cycle stability performance of catalysts in different reports are compared. It is not difficult to find that the performance of the catalyst has been improved through optimization. The catalysts were also characterized by FTIR (Fig. 3c), and no obvious difference among the catalysts was found.

Considering that the acidity of the catalyst and the amount of acidic sites are the key factors affecting cellulose depolymerization to prepare ML [37], the acidities of the catalysts were measured by NH_3-TPD, from which the temperature of NH_3 desorption and the resulting peak area reflected the acidity and the number of acidic sites, respectively. As shown in Fig. 3d–a small peak at 544.7 °C with an area of 5587 was found for CoS_2, while the peak position and its area respectively moved to higher temperature and became larger from CoS_2, to $Ni_{0.25}Co_{0.75}S_2$, to $Ni_{0.33}Co_{0.67}S_2$, and to $Ni_{0.50}Co_{0.50}S_2$, indicating that the doping of Ni increased both the acidity of CoS_2 and the number of acidic sites. Further increasing the ratio of Ni/Co from 1, to 2, and to 3, the peak position and its area respectively moved to lower temperature and became smaller from $Ni_{0.50}Co_{0.50}S_2$, to $Ni_{0.67}Co_{0.33}S_2$, to $Ni_{0.75}Co_{0.25}S_2$, and to NiS_2. Legitimately, when the ratio of Ni/Co is 1, a larger peak at 564.3 °C with an area of 7678 was found for $Ni_{0.50}Co_{0.50}S_2$, indicating that $Ni_{0.50}Co_{0.50}S_2$ has the most acidic sites and the strongest acidity

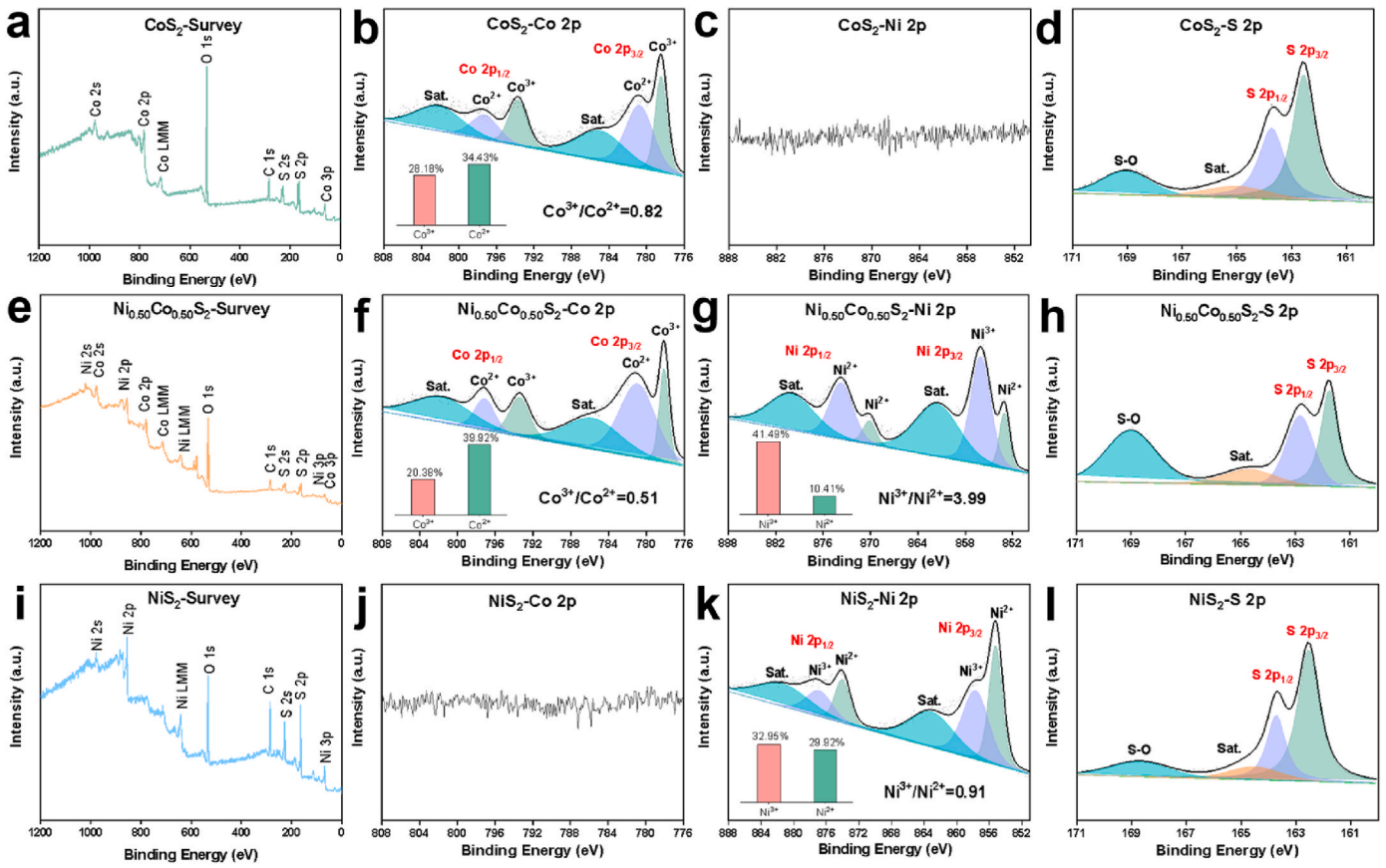

Fig. 4. XPS survey spectra of the CoS_2 (a), $Ni_{0.50}Co_{0.50}S_2$ (e) and NiS_2 (i); Co 2p XPS spectra of CoS_2 (b), $Ni_{0.50}Co_{0.50}S_2$ (f) and NiS_2 (j); Ni 2p XPS spectra of CoS_2 (c), $Ni_{0.50}Co_{0.50}S_2$ (g) and NiS_2 (k), and S 2p XPS spectra of CoS_2 (d), $Ni_{0.50}Co_{0.50}S_2$ (h) and NiS_2 (l).

Table 5
The XPS analysis results of the seven catalysts for Co 2p and Ni 2p.

Sample	Co^{3+} (%)		Co^{2+} (%)		Co^{3+}/Co^{2+}	Ni^{3+} (%)		Ni^{2+} (%)		Ni^{3+}/Ni^{2+}
	2p 1/2	2p 3/2	2p 1/2	2p 3/2		2p 1/2	2p 3/2	2p 1/2	2p 3/2	
CoS_2	11.90	16.28	9.57	24.86	0.82	[a]NA	NA	NA	NA	NA
$Ni_{0.25}Co_{0.75}S_2$	10.18	19.88	11.37	25.51	0.81	8.13	31.75	7.19	17.79	1.59
$Ni_{0.33}Co_{0.67}S_2$	9.98	13.35	10.88	23.31	0.68	11.85	28.28	5.84	14.91	1.94
$Ni_{0.50}Co_{0.50}S_2$	9.45	10.93	7.64	32.28	0.51	15.72	25.78	3.75	6.65	3.99
$Ni_{0.67}Co_{0.33}S_2$	8.54	14.36	14.86	25.90	0.56	14.90	27.96	3.96	6.98	3.92
$Ni_{0.75}Co_{0.25}S_2$	8.39	20.92	12.68	17.78	0.96	11.77	15.86	8.14	14.65	1.21
NiS_2	NA	NA	NA	NA	NA	8.96	23.99	8.59	21.33	1.10

[a] **NA = Not Available.**

compared with the other six catalysts (Table 4). The differences of acid sites and acidity between catalysts may be closely related to the valence states of transition metal elements in the catalysts, thus the XPS performance of the catalysts were tested [38].

The XPS survey of the catalysts were showed in Fig. S2. The peaks of Ni 2s, Co 2s, Ni 2p, Co 2p, O 1s, C 1s, S 2s, S 2p, Ni 3p and Co 3P were found in the XPS survey spectra. In addition, Co 2p, Ni 2p, and S 2p spectra of the three typical catalysts (CoS_2, $Ni_{0.50}Co_{0.50}S_2$ and NiS_2) were exhibited in Fig. 4, and the other catalysts can be found in Fig. S3. The Co 2p spectrum was deconvoluted into Co^{3+} at 778.7 eV (2p 3/2) and 793.8 eV (2p 1/2), Co^{2+} at 780.6 eV (2p 3/2) and 796.1 eV (2p 1/2), and satellite peaks at 784.3 eV (2p 3/2) and 802.8 eV (2p 1/2) [39]. In addition, the Ni 2p spectrum was deconvoluted into Ni^{3+} at 853.4 eV (2p 3/2) and 870.7 eV (2p 1/2), Ni^{2+} at 780.6 eV (2p 3/2) and 796.1 eV (2p 1/2), and satellite peaks at 762.1 eV (2p 3/2) and 879.4 eV (2p 1/2) [40]. Furthermore, the S 2p spectrum was deconvoluted into S^{2-} at 162.5 eV (2p 3/2), and 163.7 eV (2p 1/2), the S–O bond energy corresponds to 169 eV, and satellite peaks at 165.0 eV [39]. The chemical valence of Co 2p and Ni 2p as well as the corresponding ratio in each catalyst were listed in Table 5. The valence of Co^{2+} has been reported to favor the acid hydrolysis of cellulose to ML [28]. Interestingly, XPS results showed that the ratio of Co^{3+}/Co^{2+} decreased first and then increased with the increase of the amount of Ni doped into CoS_2. The ratio of surface Co^{3+}/Co^{2+} in $Ni_{0.50}Co_{0.50}S_2$ was only 0.51, while those in CoS_2 and $Ni_{0.75}Co_{0.25}S_2$ were 0.82 and 0.96, respectively. In addition, XPS results showed that the ratio of Ni^{3+}/Ni^{2+} increased first and then decreased with the increase of the amount of Ni doped into CoS_2. The ratio of surface Ni^{3+}/Ni^{2+} in $Ni_{0.50}Co_{0.50}S_2$ was 3.99, while those in $Ni_{0.25}Co_{0.75}S_2$ and NiS_2 were 1.59 and 0.91, respectively. The above results suggested the improved catalytic performance of $Ni_{0.50}Co_{0.50}S_2$ was potentially due to the synergistic effect of lower Co^{3+}/Co^{2+} ratio and larger Ni^{3+}/Ni^{2+} ratio.

4. Conclusion

In summary, the nickel cobalt sulfides with different molar ratios of Ni to Co were synthesized by a simple one-step hydrothermal method for the highly efficient catalytic preparation of ML from cellulose. Interestingly, with the continuous incorporation of Ni, the catalytic efficiency of the catalyst increased first and then decreased. It was worth mentioning that when the ratio of Co/Ni is 1, the ML yield was the highest (39.6 wt%), much higher than CoS_2 and NiS_2 (30.5 and 30.1 wt %, respectively). Furthermore, the characterization results of NH_3-TPD and XPS demonstrated that different Ni/Co ratios affected the number of acidic sites on the catalyst surface and the chemical valence states of Ni and Co in the catalyst, and these changes further affected the yield of ML from cellulose depolymerization. The above results also suggested the improved catalytic performance of $Ni_{0.50}Co_{0.50}S_2$ was potentially due to the synergistic effect of lower Co^{3+}/Co^{2+} ratio (0.51) and larger Ni^{3+}/Ni^{2+} ratio (3.99). Last but not least, the $Ni_{0.50}Co_{0.50}S_2$ catalyst had great recycling performance, which still maintained 78% of the initial catalytic efficiency after reused for 5 times.

Data availability

Data will be made available on request.

CRediT authorship contribution statement

Gang Wu: Formal analysis, Investigation, Methodology, Writing – original draft. **Ke Wang:** Data curation, Formal analysis. **Shasha Liu:** Data curation, Formal analysis, Funding acquisition. **Shanshan Yan:** Data curation, Investigation, Resources. **Kuan Ding:** Formal analysis, Funding acquisition. **Electo Eduardo Silva Lora:** Validation, Writing – review & editing. **Yusuf Makarfi Isa:** Resources, Writing – review & editing. **Yong Huang:** Conceptualization, Supervision, Validation, Writing – review & editing. **Shu Zhang:** Funding acquisition, Supervision, Writing – review & editing.

Declaration of competing interest

The authors declare that they have no known competing financial interests or personal relationships that could have appeared to influence the work reported in this paper.

Acknowledgements

This work was financially supported by National Natural Science Foundation of China (Grants No. 52276200 and 52106251), the Natural Science Foundation of the Jiangsu Higher Education Institutions of China (23KJB480005), and the Foundation of State Key Laboratory of Coal Combustion (Grants No. FSKLCCA2304), and Beidou Scientific Research Program of Nanjing Polytechnic Institute (NJPI-RC-2023-13).

Appendix A. Supplementary data

Supplementary data to this article can be found online at https://doi.org/10.1016/j.renene.2024.120178.

References

[1] S. Liu, G. Wu, Y. Gao, B. Li, Y. Feng, J. Zhou, X. Hu, Y. Huang, S. Zhang, H. Zhang, Understanding the catalytic upgrading of bio-oil from pine pyrolysis over CO2-activated biochar, Renew. Energy 174 (2021) 538–546.
[2] Z. Shu, Z. Kan, L. Bin, S. Hojae, H. Yong, Key considerations on the industrial application of lignocellulosic biomass pyrolysis toward carbon neutrality, Engineering (2023), https://doi.org/10.1016/j.eng.2023.02.015.
[3] L. Shasha, W. Gang, Z. Lei, H. Yong, Z. Jianbin, Z. Shu, Catalytic pyrolysis of pine sawdust over activated carbon-supported Fe for phenol-rich bio-oil, J. Anal. Appl. Pyrol. 171 (2023) 105959.
[4] Y. Shanshan, C. Haoran, Z. Haonan, L. Zixiang, W. Gang, G. Wenran, Z. Hong, H. Xun, Z. Junjie, Z. Shu, Z. Shoujun, W. Yinlong, Enhanced adsorption of bio-oil on activated biochar in slurry fuels and the adsorption selectivity, Fuel 338 (2022) 127224.
[5] S. Wang, G. Dai, H. Yang, Z. Luo, Lignocellulosic biomass pyrolysis mechanism: a state-of-the-art review, Prog. Energy Combust. Sci. 62 (2017) 33–86.
[6] G. Wu, C. Shen, S. Liu, Y. Huang, S. Zhang, H. Zhang, Research progress on the preparation and application of biomass derived methyl levulinate, Green Chem. 23 (2021) 9254–9282.
[7] J. Sun, S. Shao, X. Hu, X. Li, H. Zhang, Synthesis of oxygen-containing precursors of aviation fuel via carbonylation of the aqueous bio-oil fraction followed by C-C coupling, ACS Sustain. Chem. Eng. 10 (2022) 11030–11040.
[8] J.S. Luterbacher, D.M. Alonso, J.A. Dumesic, Targeted chemical upgrading of lignocellulosic biomass to platform molecules, Green Chem. 16 (2014) 4816–4838.
[9] Z. Liu, L. Li, C. Liu, A. Xu, Saccharification of cellulose in the ionic liquids and glucose recovery, Renew. Energy 106 (2017) 99–102.
[10] J.D. Murillo, M. Moffet, J.J. Biernacki, S. Northrup, High-temperature molecular dynamics simulation of cellobiose and maltose, AIChE J. 61 (2015) 2562–2570.
[11] K.N. Sorokina, O.P. Taran, T.B. Medvedeva, Y.V. Samoylova, A.V. Piligaev, V. N. Parmon, Cellulose biorefinery based on a combined catalytic and biotechnological approach for production of 5-HMF and ethanol, ChemSusChem 10 (2017) 562–574.
[12] C. Liu, Y.-C. Hu, Z. Yu, G. Li, A. Wang, Y. Cong, X. Wang, N. Li, Production of aviation fuel range quadricyclane with 2,5-hexanedione, ACS Sustain. Chem. Eng. 10 (2022) 17221–17229.
[13] G. Wang, Y. Meng, J. Zhou, L. Zhang, Selective hydrothermal degradation of cellulose to formic acid in alkaline solutions, Cellulose 25 (2018) 5659–5668.
[14] L. Jiang, J. Luo, F. Xu, L. Qian, Y. Wang, H. Li, Z. Fang, High yield production of levoglucosan via catalytic pyrolysis of cellulose at low temperature, Fuel 323 (2022) 124369.
[15] J. Wang, H. Cui, Y. Wang, R. Zhao, Y. Xie, M. Wang, W. Yi, Efficient catalytic conversion of cellulose to levulinic acid in the biphasic system of molten salt hydrate and methyl isobutyl ketone, Green Chem. 22 (2020) 4240–4251.
[16] A.S. Khan, Z. Man, M.A. Bustam, C.F. Kait, A. Nasrullah, Z. Ullah, A. Sarwono, P. Ahamd, N. Muhammad, Dicationic ionic liquids as sustainable approach for direct conversion of cellulose to levulinic acid, J. Clean. Prod. 170 (2018) 591–600.
[17] Y.-B. Huang, T. Yang, Y.-T. Lin, Y.-Z. Zhu, L.-C. Li, H. Pan, Facile and high-yield synthesis of methyl levulinate from cellulose, Green Chem. 20 (2018) 1323–1334.
[18] W. Gong, Y. Liu, H. Li, Y. Cui, Metal-organic frameworks as solid Bronsted acid catalysts for advanced organic transformations, Coord. Chem. Rev. 420 (2020) 213400.
[19] J. Li, X. Liang, Magnetic solid acid catalyst for biodiesel synthesis from waste oil, Energy Convers. Manag. 141 (2017) 126–132.
[20] T. Parangi, M.K. Mishra, Solid acid catalysts for biodiesel production, Comments Mod. Chem. 40 (2020) 176–216.
[21] M.A. Hanif, S. Nisar, U. Rashid, Supported solid and heteropoly acid catalysts for production of biodiesel, Catal. Rev. Sci. Eng. 59 (2017) 165–188.
[22] L. Kubie, M.S. Martinez, E.M. Miller, L.M. Wheeler, M.C. Beard, Atomically thin metal sulfides, J. Am. Chem. Soc. 141 (2019) 12121–12127.
[23] R. Ramachandran, M. Saranya, P. Kollu, B.P.C. Raghupathy, S.K. Jeong, A. N. Grace, Solvothermal synthesis of Zinc sulfide decorated Graphene (ZnS/G) nanocomposites for novel Supercapacitor electrodes, Electrochim. Acta 178 (2015) 647–657.
[24] J.-C. Xing, Y.-L. Zhu, Q.-W. Zhou, X.-D. Zheng, Q.-J. Jiao, Fabrication and shape evolution of CoS2 octahedrons for application in supercapacitors, Electrochim. Acta 136 (2014) 550–556.
[25] D.S. Ashby, J.S. Horner, G. Whang, A.S. Lapp, S.A. Roberts, B. Dunn, I. V. Kolesnichenko, T.N. Lambert, A.A. Talin, Understanding the electrochemical performance of FeS2 conversion cathodes, Acs Appl. Mater. Inter. 14 (2022) 26604–26611.
[26] T. Sun, Z. Li, X. Liu, L. Ma, J. Wang, S. Yang, Facile construction of 3D graphene/MoS2 composites as advanced electrode materials for supercapacitors, J. Power Sources 331 (2016) 180–188.
[27] S. Ravi, C.V.V.M. Gopi, H.J. Kim, Enhanced electrochemical capacitance of polyimidazole coated covellite CuS dispersed CNT composite materials for application in supercapacitors, Dalton Trans. 45 (2016) 12362–12371.
[28] G. Wu, H. Yang, W. Gao, K. Wang, M.V. Penzik, A.N. Kozlov, B. Li, Y. Huang, S. Zhang, H. Zhang, The importance of cobalt disulfide morphology for cellulose depolymerization: hydrogenolysis versus acid catalysis, J. Anal. Appl. Pyrol. 167 (2022) 105659.
[29] M. Wang, L. An, M. Wu, S. Zhang, Y. Feng, X. Zhang, J. Mi, Self-template synthesis of nickel cobalt sulfide hollow nanotubes for high-performance battery-type supercapacitors, J. Electrochem. Soc. 168 (2021) 060510.
[30] F. Wang, D. Dreisinger, M. Jarvis, T. Hitchins, L. Trytten, CO2 mineralization and concurrent utilization for nickel conversion from nickel silicates to nickel sulfides, Chem. Eng. J. 406 (2021) 126761.
[31] W. Gao, G. Wu, X. Zhu, G. Lin, X. Hu, Y. Huang, S. Zhang, H. Zhang, M.A. Akhtar, Production of methyl levulinate from cellulose over cobalt disulfide: the importance of the crystal facet (111), Bioresour. Technol. 347 (2022) 126436.
[32] W. Haiying, W. Tongtong, L. Licheng, Z. Tingwei, S. Farzad, J. Yongcan, X. Huining, Morphological effect of ceria-supported platinum catalyst on low-temperature ethylene oxidation, Appl. Catal. B Environ. 324 (2022) 122242.
[33] S. Yang, H. Shen, F. Cheng, C. Wu, Y. Cao, S. Zhuo, Q. Zhang, H. Zhang, Organometallic precursor induced defect-enriched mesoporous CeO(2)with high specific surface area: preparation and catalytic performance, J. Mater. Chem. A 8 (2020) 14006–14014.

[34] J. Zhang, Y. Liu, C. Sun, P. Xi, S. Peng, D. Gao, D. Xue, Accelerated hydrogen evolution reaction in CoS2 by transition-metal doping, ACS Energy Lett. 3 (2018) 779–786.
[35] C. Karakaya, N. Solati, U. Savaci, E. Kele, S. Turan, S. Celebi, S. Kaya, Mesoporous thin-film NiS2 as an idealized pre-electrocatalyst for a hydrogen evolution reaction, ACS Catal. 10 (2020) 15114–15122.
[36] Z. Li, R. Sun, Z. Qin, X. Liu, C. Wang, S. Lu, Y. Zhang, H. Fan, Coupling of ReS2 nanosheet arrays with hollow NiCoS4 nanocubes enables ultrafast Na+ diffusion kinetics and super Na+ storage of a NiCoS4@ReS2 heterostructure, Mater. Chem. Front. 5 (2021) 7540–7547.
[37] D. Ding, J. Xi, J. Wang, X. Liu, G. Lu, Y. Wang, Production of methyl levulinate from cellulose: selectivity and mechanism study, Green Chem. 17 (2015) 4037–4044.
[38] J. He, C. Pei, Y. Yang, B. Lai, Y. Sun, L. Yang, The structural design and valence state control of cerium-based metal-organic frameworks for their highly efficient phosphate removal, J. Clean. Prod. 321 (2021) 128778.
[39] Y.S. Kim, G.-H. Lee, B. Ju, D.-W. Kim, TCNQ-derived N/S dual-doped carbon cube electrocatalysts with built-in CoS2 nanoparticles for high-rate lithium-oxygen batteries, Chem. Eng. J. 418 (2021) 129367.
[40] Y. Shen, K. Zhang, B. Chen, F. Yang, K. Xu, X. Lu, Enhancing the electrochemical performance of nickel cobalt sulfides hollow nanospheres by structural modulation for asymmetric supercapacitors, J. Colloid Interface Sci. 557 (2019) 135–143.